Morphology and Ionization of the Interstellar Cloud Surrounding the Solar System

Priscilla C. Frisch

The first encounter between the sun and the surrounding interstellar cloud appears to have occurred 2000 to 8000 years ago. The sun and cloud space motions are nearly perpendicular, an indication that the sun is skimming the cloud surface. The electron density derived for the surrounding cloud from the carbon component of the anomalous cosmic ray population in the solar system and from the interstellar ratio of Mg^+ to Mg^0 toward Sirius support an equilibrium model for cloud ionization (an electron density of 0.22 to 0.44 per cubic centimeter). The upwind magnetic field direction is nearly parallel to the cloud surface. The relative sun-cloud motion indicates that the solar system has a bow shock.

The solar system is located in a tenuous interstellar cloud that appears to be part of the remnant gas associated with the superbubble seen around the Scorpius-Centaurus Association (*1–3*). Because the youngest supernova remnant in this star-forming region is about 250,000 years old (*4*) and the cooling time (~10^4 years) is shorter than the recombination time (~10^6 years) in ionized low-density 10,000-K gas, nonequilibrium ionization conditions could prevail in the surrounding cloud, invalidating efforts to determine the electron density from absorption line ratios.

The surrounding interstellar cloud constitutes the environment of the solar system, modifying the structure of the heliopause region (*5*) and the terrestrial magnetosphere and possibly influencing the terrestrial climate (*6*). As the sun moves through the surrounding cloud, external ions are excluded from the solar system by the compressed solar wind plasma in the heliopause region near 100 astronomical units (AU), but cloud neutrals penetrate to the inner solar system where H^0 and He^0 are ionized mainly by charge exchange with solar-wind ions and by photoionization with solar photons. These interstellar neutrals fed into the solar system by the surrounding cloud provide ~98% of the diffuse mass in the interplanetary region (*7*). Recently it was discovered that interstellar carbon, nitrogen, and oxygen, ionized by charge exchange in the inner solar system, are captured by the terrestrial magnetosphere (*6*). These captured ions provide the first significant evidence that interstellar matter (ISM) directly impacts the terrestrial system. Over the last several million years, the solar system has traversed a region of space devoid of ISM and appears to have only recently encountered the surrounding interstellar cloud (*2, 3*). In this report, data are presented to "map" the morphology of the surrounding interstellar cloud and to provide evidence that this cloud is in ionization equilibrium. These data support the view that the surrounding cloud is a quiescent remnant of the Scorpius-Centaurus superbubble, with the last ionizing event occurring over 1 million years ago.

Cosmic-ray and stellar spectral data from seven operational scientific spacecraft [Voyager 1 and Voyager 2, the Hubble Space Telescope, Ulysses, the International Ultraviolet Explorer (IUE), the Extreme Ultraviolet Explorer (EUVE), and the Roentgen Satellite (ROSAT)] were used to derive the conclusions in this report. These spacecraft are now orbiting throughout the solar system, and they demonstrate the advantage of combining data from interplanetary and Earth-orbiting spacecraft. The Voyager data were acquired at about 20 to 25 AU, the Ulysses data near 5 AU, whereas the Hubble, IUE, ROSAT, and EUVE telescopes are at 1 AU. This unique perspective on the interstellar cloud surrounding the solar system, which results from the combination of inner solar system and outer solar system data, can be further enriched with in situ data from spacecraft such as the proposed Interstellar Probe (*8*).

The relative geometry of the surrounding interstellar cloud (SIC) (*9*) and the solar system can be derived from the hydrogen column density through this cloud, the cloud velocity vector, the assumption that at the solar position the cloud velocity vector is perpendicular to the cloud surface, and the assumption that this surface is a plane. (The cloud velocity vector is derived from interstellar absorption lines in the spectra of nearby stars and observations of interstellar hydrogen and helium in the solar system.) The relative velocity vector of the cloud with respect to the sun in the local standard of rest (LSR) immediately yields intriguing results. The sun moves toward an apex position $\ell = 51°$, $b = 23°$ at 15.4 km s^{-1} (*10*). In the LSR, the surrounding cloud velocity vector $V = -19.5$ km s^{-1}, $\ell = 325.5°$, and $b = +3.6°$ if we use Ulysses observations of He^0 atoms in the outer solar system (*11*), or $V = -19.0$ km s^{-1}, $\ell = 334.5°$, $b = -1.8°$ if we use Ca^+ data toward 12 nearby stars (*2, 3*) [using data from (*12, 13*)]. Small localized samples of stars indicate that there is a velocity gradient between the upwind and downwind directions for the gas in the nearest 10 to 20 pc (*2, 3, 12, 13*). However, because the database is small and the gradient is on the order of the errors in velocity (1 to 3 km s^{-1}), I will use the global vector, which is essentially an average of the upwind and downwind values. It is easily seen that the LSR cloud vector is nearly perpendicular to the solar motion (angular separation of ~80° to 90°), implying that the sun is skimming the cloud surface, because the column densities in the antiapex directions are low (<10^{18} cm^{-2}). If the cloud velocity vector is perpendicular to the surface (parallel to a surface normal), then the local magnetic field lines, which point toward $\ell \sim 70°$ (*14*), are parallel to the cloud surface in this geometry.

If information about the distance to the cloud surface is added, then the time of the initial solar encounter with this cloud can be estimated. The total hydrogen column density [$N(H) = N(H^0) + N(H^+)$] can be derived from Mg^+ column densities in the spectra of nearby stars because Mg^+ traces both warm neutral and ionized hydrogen. (In principle, the H^0 column density can be measured directly from the Lyα absorption line; however, column densities of H^+ must be inferred from ion absorption lines.) An average value

$$A[Mg^+] \equiv N(Mg^+)/N(H) \sim 10^{-5.48} \quad (1)$$

is found toward the stars Capella, Procyon, and η UMa (see Table 1). Toward η UMa, 29% of the hydrogen is ionized, giving $N(Mg^+)/N(H^0 + H^+) = 10^{-5.49}$. Applying this ratio to the gas toward Capella and Procyon [where other estimates for $N(H^+)$ are not available] suggests that <20% of the gas is ionized toward these two stars.

Toward Sirius, two blended interstellar Mg^+ and Fe^+ absorption features are detected by the Hubble Space Telescope's Goddard High-Resolution Spectrograph (GHRS), corresponding to two interstellar clouds, with the component at 18.7 km s^{-1} corresponding to the surrounding cloud velocity (*15*). Applying the ratio $A[Mg^+] = 10^{-5.48}$ to the local Mg^+ component in Sirius gives a total hydrogen column density $N(H^0 + H^+) = N(Mg^+)/A[Mg^+] = 10^{17.71}$ cm^{-2}; for both Sirius clouds, $N(H^0 + H^+) = 10^{17.89}$ cm^{-2} (Table 1). The low total hydrogen column density for the Sirius sight line is consistent with the low value, $N(H^0) = 10^{17.85}$ cm^{-2}, seen toward the white dwarf pair RE0457-281 and RE0503-289 (*16*), ϵ CMa [$N(H^0) = 10^{18.00}$ cm^{-2} (*17*)], and Procyon [$N(H^0) = 10^{18.08}$ cm^{-2} (*18*)], all within ~25° of the Sirius sight

Department of Astronomy and Astrophysics, University of Chicago, Chicago, IL 60637, USA.

line. The apex of solar motion is directed toward $\ell = 51°$, $b = 23°$, and Sirius ($\ell = 227°$, $b = -9°$) is located in the antiapex direction. Sirius is viewed through the solar wake because the opening angle of the solar wake is ~42° (*19*). The low column densities in the antiapex direction indicate that the sun has recently encountered the surrounding cloud.

On the basis of these assumptions, the morphology of the cloud surrounding the solar system is shown in Fig. 1. The distance to the cloud surface in the Sirius sight line is given by

$$D_s = N(H^0 + H^+)/n_{tot} \qquad (2)$$

where $n_{tot} = n(H^0) + n(H^+) = n(H^0) + n_e$ for the local cloud component. The electron density is $n_e = 0.22$ to $0.44\ cm^{-3}$ (see below). If we take $N(H^0 + H^+) = 10^{17.71}\ cm^{-2}$ and $n(H^0) = \langle n(H^0) \rangle = 0.1\ cm^{-3}$, this gives $D_s = 0.3$ to 0.5 pc for the current distance to the cloud surface in the Sirius direction. If we consider this as a two-dimensional geometry with the cloud surface perpendicular to the plane of the galaxy (which is approximately correct because the LSR upwind vector has $b \sim 0°$), then the distance to the cloud surface along a surface normal (D_n), for the current epoch, is $D_n = D_s \cos(\theta) = 0.05$ to 0.16 pc. For elapsed time since the sun-cloud encounter t_e,

$$D_n = t_e[V_{sun}\cos(\phi + \theta) + V_{lisw}] \qquad (3)$$

where V_{sun} is the LSR solar velocity vector ($V_{sun} \sim 15.4\ km\ s^{-1}$), and V_{lisw} is the LSR cloud vector ($V_{lisw} = -19.0\ km\ s^{-1}$, $\ell = 334.5°$, $b = -1.8°$). The angle $\theta \sim 72.5°$ is the separation between the Sirius sight line and cloud surface normal; $\phi \sim 4°$ is the separation between Sirius ($\ell = 227°$) and the antiapex direction in this two-dimensional model. These angles and line segments are illustrated in Fig. 1.

Solving these equations gives $t_e = 2000$ to 8000 years as the time since the initial encounter of the solar system with the surrounding cloud for $n_e = 0.22$ to $0.44\ cm^{-3}$ and $n(H^0) = 0.05$ to $0.2\ cm^{-3}$, including the uncertainties in the surrounding cloud velocity vector. Because the sun appears to be skimming the cloud surface, the encounter epoch is sensitive to uncertainties in the cloud velocity vector and the assumed value for $n(H^0)$ in the SIC (*20*). The hatched region in Fig. 1, representing the cloud surrounding the solar system, is not homogeneous because there are two velocity features in front of the nearest star, α Cen A ($d = 1.3$ pc, and near the upwind direction) (*21*). There are three velocity features toward α Aql ($d = 5$ pc) (*12, 13*) and two toward Sirius (*15*). The second interstellar cloud seen toward Sirius, the cloud containing most of the sight-line ISM toward Capella, and multiple components in the hatched region ISM are not illustrated.

The cloud morphology in Fig. 1 presents the essential characteristics of the cloud surrounding the solar system, and it is expected that this morphology will be updated and modified as additional data on cloud multiplicity become available. If the uncertainties in the data used in constructing Fig. 1 can be reduced, it may be possible to determine with precision the encounter epoch and therefore to establish whether relatively low-density interstellar clouds are capable of affecting the terrestrial climate.

Voyager 1 and Voyager 2 spacecraft in situ data on the carbon component of the anomalous cosmic ray (ACR) population (*22*) can be used to corroborate the electron density in the surrounding cloud found from Hubble Space Telescope GHRS Mg^+ and Mg^0 data in the spectra of the nearby star Sirius A (*15*). The ACR results are consistent with the Sirius A results, which are derived from a sight line 50,000 times longer. The consistency of results derived from these two independent analyses provides evidence that the underlying model of ionization equilibrium is correct.

When the trace elements in an interstellar cloud are in ionization equilibrium, that is, the rate of ionization and recombination events are equal

$$\Gamma(X^n)n(X^n) = \alpha(X^{n+1})n(X^{n+1})n_e \qquad (4)$$

Here, $\Gamma(X^n)$ is the total ionization rate for X^n (per second), $\alpha(X^{n+1})$ is the total rate for the combination of X^{n+1} with an electron to form X^n, and $n(X)$ and n_e are the spatial densities (per cubic centimeter) for species X and electrons, respectively. At these densities, Mg^0 and C^0 ionization are dominated by photoionization (although the charge-exchange rate for C^0 is poorly known) (*23*). It is generally assumed that $N(X) = L\, n(X)$, where L is the path length through the interstellar cloud and $N(X)$ is the column density (per square centimeter). Equation 4 has been applied previously to interstellar Mg^0 absorption lines in the spectra of Sirius A ($d = 2.7$ pc, $\ell = 227°$, $b = -9°$), giving $n_e \sim 0.09$ to $0.39\ cm^{-3}$ for cloud temperature $T = 7000$ to 8000 K (*15*). However, these high values have been unconfirmed.

In the solar system, neutral carbon is found in the ACR population, with abundances indicating a source population ratio $N(C^0)/N(O^0) = 0.0039\ (+0.0039, -0.0020)$ (*22*). The source population is believed to be neutral interstellar atoms, which penetrate the solar wind plasma and, after ionization, are accelerated to cosmic ray energies within the solar system (*24*). In order to derive the source population ratio from the observed ACR

Table 1. Properties of the surrounding interstellar cloud toward nearby stars. The Sirius, Capella, and Procyon values are based on Hubble Space Telescope GHRS data. The η UMa values are based on Copernicus and IUE data (*2, 3*). Values for $N(H^0 + H^+)$ enclosed in brackets are inferred from Mg^+ abundances (see text). The projected lisw vectors in the directions of these stars are as follows: Sirius, 19.5 km s^{-1}; Capella, 21.9 km s^{-1}; Procyon, 19.5 km s^{-1}; η UMa, −5.8 km s^{-1}.

Element	Column density (cm^{-2})	Heliocentric velocity (km s^{-1})	Cloud temperature (K)
	*Sirius (α CMa) component 1 (SIC), d = 2.7 pc, ℓ = 227°, b = −9°**		
N(HI + HII)	[5.10×10^{17}]§		7600 ± 3000
HI	[$0.9–1.6 \times 10^{17}$]‖		
MgII	1.65×10^{12}	18.7 ± 1.5	
	*Sirius α CMa component 2**		
N(HI + HII)	[$2.4–3.0 \times 10^{17}$]§		1000^{+6000}_{-1000}
MgII	9.0×10^{11}	13.0 ± 1.5	
	Capella (α Aur) d = 12 pc, ℓ = 163°, b = +5°†		
N(HI + HII)	[2.0×10^{18}]§	21.7–22.5	7000 ± 200
HI	$1.65–1.8 \times 10^{18}$		
MgII	6.5×10^{12}	21–23	
	Procyon (α CMi) d = 3.5 pc, ℓ = 214°, b = +13°†		
N(HI + HII)	[1.1×10^{18}]§	22.0	6700 ± 200
HI	$1.15–1.2 \times 10^{18}$		
MgII	3.47×10^{12}	21.2	
	Alcaid (η UMa) d = 42 pc, ℓ = 101°, b = +65°‡		
N(HI + HII)	1.0×10^{18}		
HI	7.1×10^{17}		
MgII	3.2×10^{12}	3.9–8.3	

*Data from Lallement *et al.* (*15*). The "surrounding cloud" component refers to the cloud surrounding the solar system, and the blue-shifted cloud is more distant. †Data from Linsky *et al.* (*18*). ‡The H^0 column densities are from York (*35*), and the H^+ column densities are from (*2*). The Mg^+ column densities are based on IUE data of Frisch *et al.* (*3*). Vallerga *et al.* (*36*) found a velocity for the Ca^+ K line of −2.8 km s^{-1}, which is intrinsically more accurate than the IUE velocities shown in the table. §The $N(H^0 + H^+)$ value is calculated using the η UMa ratio $N(Mg^+)/N(H^0 + H^+) = 10^{-5.49}$ [η UMa is the only star in the table for which both $N(H^0)$ and $N(H^+)$ are available]. However, this abundance is also equal to the average Mg^+ abundance for Capella, Procyon, and η UMa. ‖The two values of $N(H^0)$ are calculated using the range $n_e = 0.22$ to $0.44\ cm^{-3}$ found locally, combined with a nominal local density of $n(H^0) = 0.1\ cm^{-3}$, giving $n_e + n(H^0) = 0.32$ to $0.54\ cm^{-3}$.

N(C)/N(O) ratio, the observed ratio is corrected for ionization by solar ultraviolet photons, charge-exchange reactions in the heliopause region and with the solar wind, and the acceleration and propagation of the ions within the solar system. However, the "filtration" correction factors at the heliopause region are poorly known at present, especially for carbon, and these uncertainties are not contained in the quoted errors.

Equation 4 for the carbon equilibrium in the SIC can be rewritten as

$$\Gamma(C^0)N(C^0)/N(O^0) = \alpha(C^+)n_e N(C^+)/N(O^0)$$
$$= \alpha(C^+)n_e R_c/F(n_e) \qquad (5)$$

Here, I have used the fact that in the SIC oxygen ionization is closely coupled to hydrogen ionization through charge exchange, so that the neutral fraction, $F(n_e)$, of oxygen is the same as the fractional neutrality of hydrogen, giving

$$F(n_e) = 1 - n_e/(n_e + n(H^0)) \qquad (6)$$

where $n_e \sim n(H^+)$. Because carbon is mainly in the form C^+ in diffuse interstellar clouds such as the SIC, $N(C_{total}) \approx N(C^+)$. The cosmic abundance ratio for carbon is $R_c = N(C_{total})/N(O_{total}) = 0.427$ (*25*). In the SIC, observations of both the Lyα emission from the interplanetary glow atoms and Lyα absorption in the nearest stars give a nominal value for the average neutral hydrogen spatial density in the SIC of $\langle n(H^0)\rangle \sim 0.1$ cm^{-3} (*2, 3, 26*). In the SIC, the ratio $N(C^+)/N(O^0)$ is equal to $R_c/F(n_e)$. The ionization rate of C^0 in the cloud surrounding the sun is poorly known. I will use the ionization rate for a neutral hydrogen cloud surface $\Gamma = 1.31 \times 10^{-10}$ s^{-1} from Black and Dalgarno (*27*) (with a nominal uncertainty of a factor of 2). For a cloud temperature range T = 6700 to 8000 K, $\alpha_r(C^+) = 6.03$ to 5.40×10^{-13} cm^3 s^{-1} (*23, 28*). If $n(H^0) \approx \langle n(H^0)\rangle \sim 0.1$ cm^{-3}, Eq. 5 for the ionization equilibrium of C^0 in the SIC yields an electron density of n_e = 0.26 to 0.62 cm^{-3}, including errors in the ACR $N(C^0)/N(O^0)$ ratio and cloud temperature.

The allowable range of n_e is narrowed if the ARC and Sirius A Mg results are compared directly, using improved Mg^+ dielectronic recombination rates. The total recombination rate for Mg^+ is enhanced in the temperature range $T > 6000$ K by dielectronic recombination, and so Mg^0 is a good tracer of warm, low-density clouds such as the SIC. The charge-exchange formation of Mg^+ is insignificant, as seen in Fig. 2, which shows the electron density solution to the condition $\alpha_{ce}(T_4)n_e = \Gamma(Mg^0)$. The rates $\alpha_{ce}(T_4)n_e$ and $\Gamma(Mg^0)$ are the formation rates (per second) of Mg^+ by charge exchange and photoionization, respectively (*29*). Except for $T \approx 8000$ K and $n_e > 0.3$ cm^{-3}, where small corrections must be made, the charge exchange formation of Mg^+ is insignificant for the range of densities and temperatures calculated here. At electron densities greater than the plotted solution, both the ionization and recombination rates in $Mg^+ \leftrightarrow Mg^0$ equilibrium are proportional to the electron density, so the ratio $N(Mg^+)/N(Mg^0)$ can no longer be used to constrain the electron density.

Using the photoionization rate $\Gamma(Mg^0) = 4.0 \times 10^{-11}$ s^{-1} (*23*) and the ratio $N(Mg^+)/N(Mg^0) = 220\ (+70, -40)$ found for the SIC component by the Hubble Space Telescope GHRS (*15*) gives the electron densities shown in Fig. 3 for both the Mg and ARC data, as a function of temperature. The error envelope on the electron density as a function of temperature for the Sirius A data corresponds to the errors in the ratio. For an SIC temperature range of T = 6700 to 8000 K and $n(H^0) \sim 0.1$ cm^{-3} (Fig. 3), comparisons of the two data sets constrain the electron density to the range n_e = 0.28 to 0.43 cm^{-3}, including errors in temperature and the ACR ratio $N(C^0)/N(O^0)$. If, instead, a value $n(H^0) \sim 0.15$ cm^{-3} is used, the derived n_e is 0.33 to 0.44 cm^{-3}. The derived n_e is weakly sensitive to assumed hydrogen spatial density. Using

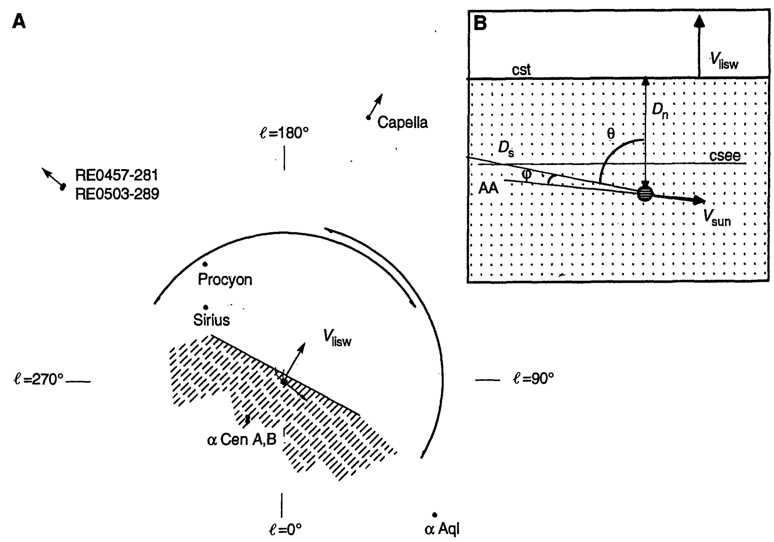

Fig. 1. Two-dimensional schematic of the closest cloud layer of the local interstellar cloud system: (**A**) the surrounding cloud and several nearby stars; (**B**) an enlargement of the region around the sun. All vectors are shown in the LSR, and the four points of the galactic coordinate system (ℓ = 0°, 90°, 180°, 270°) are labeled. "Basic" solar motion through the LSR (*10*) and an LSR cloud motion [$V = -19.0$ km s^{-1}, ℓ = 334.5°, $b = -1.8°$, (*2, 3*)] are assumed. Also, it was assumed that the total hydrogen column density in the Sirius direction is low [$N(H^0 + H^+) \sim 10^{17.71}$ cm^{-2}] and that the local cloud velocity vector is normal to the cloud surface, which is assumed to be locally a plane. In (A), the local interstellar wind vector is labeled lisw; the vector embedded in the cloud (cross-hatched region) is the solar vector, with the current position of the sun indicated by a dot. Several nearby stars are plotted at their respective galactic coordinates. The arcs indicate the angular regions containing the stars Lallement *et al.* (*12*) and Bertin *et al.* (*13*) used to derive the cloud downwind velocity vector ℓ ≈ 45° to 170° and the "low Mg II column density" region of Genova *et al.* (*34*) at b = 0°, which is centered approximately on the downwind direction ℓ ≈ 125° to 270° (in the LSR). Many nearby features are not shown (for example, cloud multiplicity toward α Cen, α Aql, and Sirius A, and most of the ISM mass toward Capella). An artist's view of the solar wake is included (small curved feature). In (B), line "cst" represents the cloud surface today, line "csee" represents the cloud surface during the encounter epoch (between the sun and cloud), V_{sun} and V_{lisw} are the solar and cloud velocity vectors, line segment AA is in the antiapex direction (the opposite direction from V_{sun}), line segment D_s is directed toward Sirius (at ℓ = 227°), and line D_n is the distance to the cloud surface along a surface normal at the current epoch. The angles θ (72.5°) and φ (4°) are not plotted to scale. The upwind magnetic field is parallel to the cloud surface (*14*). If the cloud motion is not parallel to the surface normal as is assumed, then this cloud morphology is not correct.

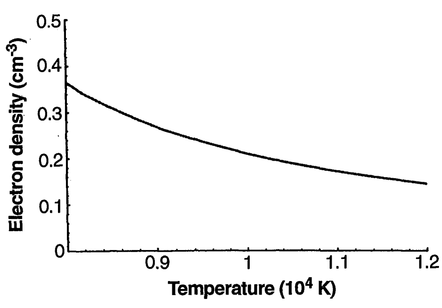

Fig. 2. The electron density for which charge-exchange ionization of Mg^0 is equal to photoionization plotted against temperature. The plotted electron density is the solution to the equation $\alpha_{ce}(T_4)n_e = \Gamma(Mg^0)$. The calculation for the rate $\alpha_{ce}(T_4)$, from Allan *et al.* (*29*) is valid in the range $0.8 < T_4 < 2.0$.

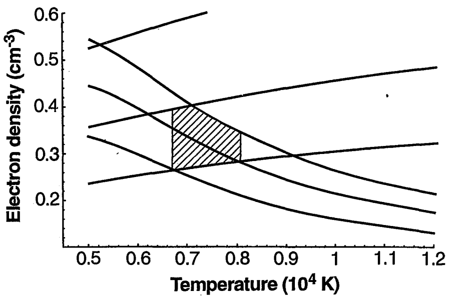

Fig. 3. Electron densities calculated from the carbon component of the ACR population compared to calculations based on $N(Mg^+)/N(Mg^0)$ toward Sirius, on the assumption that the interstellar gas surrounding the solar system is in ionization equilibrium. The magnesium-based electron density decreases as a function of temperature, whereas the carbon ARC value increases. The error bars are based on measurement errors. If errors on Γ (C^0) are also included, the independently derived values constrain the electron density in the cloud surrounding the solar system to be $n_e = 0.22$ to 0.44 cm^{-3} for $T = 6700$ to 8000 K and $n(H^0) \sim 0.1$ cm^{-3}. The coincidence in derived values is evidence that the underlying model for ionization equilibrium in this cloud is correct. The high electron density, $n_e > 0.22$ cm^{-3}, combined with an assumed magnetic field strength of $B > 0.5$ μG, indicates that the motion of the solar system through this cloud will result in a bow shock around the solar system. The cross-hatched area shows overlap in electron densities for temperature range.

nominal errors for the C^0 photoionization rate of -0.84, $+0.69 \times 10^{-10}$ s^{-1} (*30*), n_e is in the range 0.22 to 0.44 cm^{-3} for $n(H^0) \approx 0.1$ cm^{-3}.

The key point about these results is that n_e is determined independently with the use of different techniques, the only common feature being that the gas is assumed to be in ionization equilibrium. In fact, the ratios $N(Mg^+)/N(Mg^0)$ and $N(C^+)/N(C^0)$ have different temperature dependences in the range T = 5000 to 10,000 K, because the recombination rate of $Mg^+ \rightarrow Mg^0$ increases with temperature (as a result of dielectronic recombination), whereas the recombination rate of $C^+ \rightarrow C^0$ decreases with temperature (as a result of radiative recombination). These two separate estimates of n_e provide a good overlap of values at the temperature range of the SIC. The good agreement between the predictions of the ionization equilibrium model and the n_e values derived from the totally independent ACR and Sirius absorption line data provides powerful evidence in favor of the ionization equilibrium of trace elements in the surrounding interstellar cloud.

For $n(H^0 + H^+) \approx 0.3$ to 0.5 cm^{-3}, $T \approx 7000$ K, and magnetic field $B \approx 1.4$ μG (*31*), the ratio of gas to magnetic pressure is $\beta \sim 2$ to 11, and so the surrounding cloud would drag a captured galactic field through space. For larger magnetic field strengths ($B > 3.5$ μG), $\beta < 1$ and the magnetic field should confine the surrounding cloud and prevent the observed flow. If the sun has a bow shock, the observed sun-cloud relative velocity, V = 26 km s^{-1} (*2, 3, 11–13*) satisfies $V > V_f = (V_s^2 + V_a^2)^{0.5}$, where $V_s \sim 10$ km s^{-1} is the sound speed for T = 6700 to 8000 K, and $V_a \sim 2.18\, B/\sqrt{n_i}$ is the Alfven velocity (where n_i is the ion density and B is the magnetic field in microgauss), and V_f is the fast-mode magnetosonic velocity. For a nominal value for the magnetic field strength of $B \sim 1.4$ μG and $n_e = 0.2$ cm^{-3}, $V_f = 12$ km s^{-1} and a bow shock will form around the solar system as it moves through space. For $B \sim 0.5$ to 3 μG, V_f = 10.3 to 12.1 km s^{-1}. Evidently for a reasonable range of the magnetic field strength, the solar system will have a bow shock, corroborating earlier conclusions (*12, 13*). The nature of a two-shock structure around the solar system has been discussed by Baranov and associates and by Lallement *et al.* [see (*32*)].

The good overlap in the electron densities predicted by the Sirius A Mg data and the anomalous cosmic-ray C data are evidence that the SIC is in ionization equilibrium and that it is not composed of nonequilibrium recombining gas. Thus, the SIC has not been violently heated within the past million years. This conclusion agrees with the results of Bertin *et al.* (*13*), who concluded that the depletion of interstellar Ca^+ onto dust grains indicates a stable environment. It also agrees with my conclusion that the surrounding interstellar gas is residual material from a cloud evaporative phase 1 million to 5 million years ago in the Scorpius-Centaurus Association superbubble (*4*). However, in order for this conclusion that the local cloud is in ionization equilibrium to be definitive, both the filtration factors for neutrals at the heliopause and the far-ultraviolet interstellar radiation field at the solar position need to be better understood. The electron density range n_e = 0.22 to 0.44 cm^{-3} corresponds to a hydrogen fractional ionization $n_e/n(H^0 + H^+)$ of 0.69 to 0.81 for $n(H^0) = 0.1$ cm^{-3}. Models of the interface between the surrounding cloud and the postulated surrounding coronal substrate predict 42 to 54% hydrogen ionization (*33*), suggesting that additional ionization sources are required or that $n(H^0)/\langle n(H^0)\rangle$.

REFERENCES AND NOTES

1. The Scorpius-Centaurus Association is centered about 150 pc from the sun, and the superbubble features associated with this association have radii of ≥90 pc. The cloud surrounding the solar system is a few parsecs in extent in the hemisphere of the sky opposite the galactic center, but in the galactic center hemisphere (toward the Scorpius-Centaurus Association) interstellar gas with the local cloud characteristics is seen for 10 to 30 pc. Evidently the local cloud is composed of interstellar gas that has evaporated from interstellar clouds embedded in this superbubble and has been compressed by a shell-forming event ~400,000 years ago, which expanded into the evaporated gas. See (*2, 3*) for more details.
2. P. C. Frisch, *Space Sci. Rev.*, in press; *Nature* **293**, 377 (1981); ——— and D. G. York, in *The Galaxy and the Solar System*, R. Smoluchowski, J. N. Bahcall, M. Matthews, Eds. (Univ. of Arizona Press, Tucson, 1986), pp. 83–100; in *Extreme Ultraviolet Astronomy*, R. F. Malina and S. Bowyer, Eds. (Pergamon, New York, 1990), pp. 322–332.
3. P. C. Frisch, D. E. Welty, D. G. York, in preparation.
4. R. J. Borken, and D. C. Iwan, *Astrophys. J.* **218**, 511 (1977); J. Davelaar, J. A. M. Bleeker, A. J. M. Deerenberg, *Astron. Astrophy.* **92**, 231 (1980).
5. T. E. Holzer, *Annu. Rev. Astron. Astrophy.* **27**, 199 (1989).
6. Recent satellite data [Solar Anomalous and Magnetospheric Particle Explorer (SAMPAX), Interplanetary Monitoring Probe (IMP) 8, International Cometary Explorer (ICE), Cosmos] establish that interstellar gas nucleii (which have penetrated the solar system as neutral atoms and then become ionized and accelerated) are trapped in the magnetosphere of Earth (J. H. Adams *et al.*, *Astrophys. J.* **375**, L45 (1991); J. R. Cummings, *et al.*, paper SH6.2, 23rd International Cosmic Ray Conference, Calgary, Canada, 1993. The references in P. C. Frisch [*Astrophys. J.* **407**, 198 (1993)] list papers discussing postulated, but unproved, influences of interstellar gas on terrestrial climate, including scenarios with changed upper atmosphere chemistry due to the infall of interstellar gas.
7. M. A. Gruntman, *Planet. Space Sci.* **41**, 307 (1993).
8. T. E. Holzer, R. A. Mewaldt, M. Neugebauer, Collected Papers from Interstellar Probe Workshop, Ballston, VA, 20 and 21 March 1990.
9. The cloud surrounding the solar system, also known as the "local fluff" or "local interstellar cloud," is generally used to refer to gas within about 3 to 5 pc. Multiple interstellar velocity features have been found in front of the nearby stars Sirius A, α Aql, and α Cen, however (see references below). The "surrounding interstellar cloud" refers to the interstellar gas, or cloud component, immediately surrounding the solar system.
10. I am using the "basic" solar motion, given by a solar motion of velocity of 15.4 km s^{-1} toward the galactic direction $\ell = 51°$, $b = 23°$. The "basic" velocity frame of reference is defined so that the average motion of nearby K giant stars is zero. According to Mihalas and Binney, this is a more valid LSR definition than commonly used conversion vectors based on bright stars alone [D. Mihalas, and J. Binney, *Galactic Astronomy: Structure and Kinematics* (Freeman, San Francisco, 1981), p. 398].
11. M. Witte, H. Rosenbauer, M. Banaszkiewicz, H. Fahr, *Adv. Space Res.* **13** (no. 6), 121 (1993).
12. R. Lallement and P. Bertin, *Astron. Astrophy.* **266**, 479 (1992); R. Lallement *et al.*, *ibid.* **168**, 225 (1986); R. Lallement *et al.*, *Science* **260**, 1095 (1993).
13. P. Bertin, R. Lallement, R. Ferlet, A. Vidal-Madjar, *Astron. Astrophys.* **278**, 549 (1993).
14. J. Tinbergen, *ibid.* **105**, 53 (1982).
15. R. Lallement, P. Bertin, R. Ferlet, A. Vidal-Madjar, J. L. Bertaux, *ibid.*, in press. The GHRS data show that two clouds are present, separated by 5.7 ± 3.0 km s^{-1}. Both clouds contribute to the interstellar Mg^+ and Fe^+ absorption features. See Table 1.
16. S. Vennes *et al.*, *Astrophys. J.*, **421**, L35 (1993). The hydrogen column density of MCT 0455-2812 (RE0457-281) is confirmed by recent EUVE observations of the He I edge (S. Vennes, personal communication). The white dwarfs RE0457-281 and RE0503-289 are denoted MCT 0344-2812 and MCT 0501-2858, respectively, in the EUVE survey. These stars are located at d = 90 pc, ℓ = 229°, b = −36°.
17. J. V. Vallerga, P. W. Vedder, B. Y. Welsh, *Astrophys. J.* **414**, L65 (1993). The star ε CMa is located at d = 187 pc, ℓ = 240°, b = −11°.
18. J. L. Linsky *et al.*, *ibid.* **402**, 694 (1993); J. L. Linsky, A. Diplas, T. Ayres, B. Wood, A. Brown, paper presented at the 183rd American Astronomical Society meeting, Washington DC, 1994.
19. The opening angle can be approximated by the inverse tangent of the ratio of the relative sun-cloud

velocity (~26 km s^{-1}) and the speed at which the bow shock propagates in a perpendicular direction (~10 km s^{-1}). The recombining solar wind plasma and suprathermal H^0 may also be seen in the wake region. The most likely source of detection of the solar wake would be in Lyα absorption, because the H I Lyα line becomes optically thick at N(H I) ~ 10^{13} cm^{-2} for local cloud properties. A H^0 population heated in the solar system may contribute H I Lyα absorption with an anomalous velocity dispersion toward background stars such as Sirius (located close to the antiapex of solar motion, offset about 4° downwind).

20. For instance, doubling the H^0 density from 0.1 to 0.2 cm^{-3} yields t_e = 3500 to 5200 years ago for the cloud vector ($V = -19.0$ km s^{-1}, $\ell = 334.5°$, $b = -1.8°$).
21. W. B. Landsman, R. C. Henry, H. W. Moos, J. L. Linsky, *Astrophys. J.* **285**, 801 (1984).
22. A. C. Cummings, and E. C. Stone, Contributions to the 20th International Cosmic Ray Conference, Moscow, U Supl. Ser. R (1987); Contributions to the 21st International Cosmic Ray Conference, Adelaide, South Australia (1990). Because the O and C errors are correlated, they are reduced by 10% (A. C. Cummings, personal communication).
23. P. C. Frisch, D. E. Welty, D. G. York, J. R. Fowler, *Astrophys. J.* **357**, 514 (1990); J. M. Shull and M. van Steenberg, *Astrophys. J. Suppl. Ser.* **48**, 95 (1982). The recombination rate of C^+ and an electron is given by $\alpha_r(C^+) = 4.70 \times 10^{-13}\, T_4^{-0.624}$ cm^3 s^{-1}, where T_4 is the temperature in units of 10^4 K.
24. J. R. Jokipii, in *COSPAR Colloquia Series No. 1, Physics of the Outer Heliosphere*, S. Grzedzielski and E. Page, Eds. (Pergamon, New York, 1990), p. 169.
25. D. C. Morton, *Astrophys. J. Suppl. Ser.* **77**, 119 (1991).
26. J. M. Ajello *et al.*, *Astrophys. J.* **317**, 964 (1987); J. Murthy, *et al.*, *ibid.* **315**, 675 (1987); P. C. Frisch, *COSPAR Colloquia Series No. 1, Physics of the Outer Heliosphere*, S. Grzedzielski and E. Page, Eds. (Pergamon, New York, 1990), pp. 19–21; R. Lallement, *ibid.*, pp. 49–60.
27. J. H. Black and A. Dalgarno, *Astrophys. J. Suppl. Ser.* **34**, 405 (1977).
28. This temperature range is based on Ulysses spacecraft observations of the arrival angle of helium [T = 6700 ± 1500 K (*15*)] and GHRS data for interstellar gas within 1 to 12 pc (see Table 1).
29. The total recombination rate for $Mg^+ \rightarrow Mg^0$ includes radiative and dielectronic contributions. For this comparison, the magnesium-based n_e is derived from the dielectronic recombination rate for $Mg^+ \rightarrow Mg^0$ for the temperature range $1500 < T_e < 60{,}000$ K (including spin-orbit coupling, which mixes autoionizing and nonautoionizing states at low temperatures [H. Nussbaumer, and P. J. Storey, *Astron. Astrophys. Suppl. Ser.* **64**, 545 (1986)]. At $T_e \sim 6000$ K the radiative (*23*) and dielectronic recombination rates for $Mg^+ \rightarrow Mg^0$ are approximately equal, and so the uncertainty introduced by the $Mg^+ \rightarrow Mg^0$ recombination rate may be small. However, for 6500 K $< T <$ 10,000 K, this uncertainty can be significant. In the calculations of this electron density, Lallement *et al.* (*15*) used a parameterization of a dielectronic recombination by V. L. Jacobs, J. Davis, J. E. Rogerson, M. Blaha [*Astrophys. J.* **230**, 627 (1979)]. However, the lower limit of the effective range of the calculation of Jacobs *et al.* is 10,000 K, so it is inapplicable at surrounding cloud temperatures. In warm ionized nebulae, charge exchange between Mg^0 and H^+ contributes to the formation of Mg^+. This rate is calculated at $\alpha_{ce}(T_4) = 1.74 \times 10^{-9} \exp(-2.210/T_4)$ cm^3 s^{-1}, where $T_4 = T_e/10^4$, in the range $0.8 < T_4 < 2.0$ [R. J. Allan, R. E. S. Clegg, A. S. Dickinson, D. R. Flower, *Mon. Not. R. Astron. Soc.* **235**, 1245 (1988)].
30. D. Pequignot and S. M. V. Aldrovandi, *Astron. Astrophys.* **161**, 169 (1986); F. C. Bruhweiler and Y. Kondo, *Astrophys. J.* **260** L91 (1982).
31. This magnetic field strength represents the total azimuthal field derived for the ordered magnetic field component in the vicinity of the sun. See R. J. Rand and S. R. Kulkarni [*Astrophys. J.* **343**, 760 (1989)] and R. J. Rand and A. G. Lyne (in preparation).
32. V. B. Baranov, M. G. Lebedev, M. S. Ruderman, *Astrophys. Space Sci.* **66**, 441 (1979); V. B. Baranov, M. G. Lebedev, Ju. G. Malama, *Astrophys. J.* **375**, 347 (1991); R. Lallement *et al.*, *ibid.* **396**, 696 (1992).
33. J. D. Slavin, *Astrophys. J.* **346**, 718 (1989); K.-P. Cheng and F. C. Bruhweiler, *ibid.* **364**, 573 (1990).
34. R. Genova *et al.*, *ibid.* **355**, 150 (1990).
35. D. G. York, *ibid.* **204**, 750 (1976).
36. J. V. Vallerga *et al.*, *ibid.* **411**, 729 (1993).
37. I acknowledge the support of National Aeronautics and Space Administration Space Physics Division grant NAGW-2610 during the preparation of this paper. I especially thank R. Lallement and J. Linsky for sending me preprints in advance of publication.

9 February 1994; accepted 14 July 1994

Chemical Sequence Control of β-Sheet Assembly in Macromolecular Crystals of Periodic Polypeptides

Mark T. Krejchi, Edward D. T. Atkins, Alan J. Waddon, Maurille J. Fournier, Thomas L. Mason, David A. Tirrell*

A family of uniform periodic polypeptides has been prepared by bacterial expression of the corresponding artificial genes, with the objective of exploring the potential for control of supramolecular organization in genetically engineered protein-based polymeric materials. The repeating units of the polypeptides consist of oligomeric alanylglycine sequences interspersed with glutamic acid residues inserted at intervals of 8 to 14 amino acids. Crystallization of such materials from formic acid produces β-sheet structures in the solid state, as shown by vibrational spectroscopy, nuclear magnetic resonance spectroscopy, and wide-angle x-ray diffraction. The diffraction results, together with observations from electron microscopy, are consistent with the formation of needle-shaped lamellar crystals whose thickness is controlled by the periodicity of the primary sequence. These results can be used to control solid-state structure in macromolecular materials.

The design and synthesis of artificial proteins is an emerging area of research with important implications for structural biology, materials science, and biomedical engineering. Significant progress has been reported in the design of simple proteins that adopt predictable secondary structures, and preliminary successes in higher order protein folding have been achieved in several laboratories (*1*).

We are interested in controlling the solid-state structures—and in particular the crystal structures—of artificial proteins. Unlike the products of conventional polymerization processes, artificial proteins can be engineered with virtually absolute control of chain length, sequence, and stereochemical purity. Appropriately designed artificial proteins thus represent a new class of macromolecular materials, with properties potentially quite different from those of the synthetic polymers currently available and in widespread use (*2*).

Since the concept of macromolecular structure was established in the early part of this century by Staudinger (*3*), enormous effort has been devoted to the development of polymerization processes that afford improved control of chain architecture and to the elucidation of the relations between molecular structure and supramolecular organization in solid polymers. Keller and others (*4*) in the 1950s established the generality of polymer crystals as folded-chain lamellae, and it is now accepted that the folded-chain architecture is a kinetic trap for essentially any flexible polymer chain. Thus, it is prudent to focus any crystal engineering effort on lamellar structures, with the following key parameters the objects of control: (i) chain conformation, (ii) unit cell structure, (iii) lamellar thickness, and (iv) lamellar surface structure. Toward these ends, we describe herein the design, synthesis, and structural analysis of the family of artificial proteins represented by sequence 1 (Fig. 1).

The design of this simple family of sequences was based on concepts and observations drawn in part from polymer chemistry and physics and in part from structural biology. The repeating alanylglycine (AlaGly) dyads were selected to form extended β strands and to assemble into β-sheet crystal "stems" in the lamellar aggregate. Poly(AlaGly) and a variety of AlaGly-rich polypeptides (including *Bombyx mori* silk fibroin) are known to adopt β-sheet struc-

M. T. Krejchi, A. J. Waddon, D. A. Tirrell, Department of Polymer Science and Engineering, University of Massachusetts, Amherst, MA 01003, USA.
E. D. T. Atkins, H. H. Wills Physics Laboratory, University of Bristol, Tyndall Avenue, Bristol, BS8 1TL, United Kingdom.
M. J. Fournier and T. L. Mason, Department of Biochemistry and Molecular Biology, University of Massachusetts, Amherst, MA 01003, USA.

*To whom correspondence should be addressed.